Published for SISSA by Springer

Received: March 26, 2019
Accepted: June 11, 2019
Published: June 18, 2019

Continuing search for new physics in $b \to s\mu\mu$ decays: two operators at a time

Ashutosh Kumar Alok,[a] **Amol Dighe,**[b] **Shireen Gangal**[b] **and Dinesh Kumar**[c,d]

[a] *Indian Institute of Technology Jodhpur, Jodhpur 342037, India*
[b] *Tata Institute of Fundamental Research, Homi Bhabha Road, Mumbai 400005, India*
[c] *National Centre for Nuclear Research, Warsaw, Poland*
[d] *Department of Physics, University of Rajasthan, Jaipur 302004, India*

E-mail: akalok@iitj.ac.in, amol@theory.tifr.res.in, shireen.gangal@theory.tifr.res.in, Dinesh.Kumar@ncbj.gov.pl

Abstract: The anomalies in the measurements of observables involving $b \to s\mu\mu$ decays, namely R_K, R_{K^*}, P_5', and B_s^ϕ, may be addressed by adding lepton-universality-violating new physics contributions to the effective operators $\mathcal{O}_9, \mathcal{O}_{10}, \mathcal{O}_9', \mathcal{O}_{10}'$. We analyze all the scenarios where the new physics contributes to a pair of these operators at a time. We perform a global fit to all relevant data in the $b \to s$ sector to estimate the corresponding new Wilson coefficients, $C_9^{\rm NP}, C_{10}^{\rm NP}, C_9', C_{10}'$. In the light of the new data on R_K and R_{K^*} presented in Moriond 2019, we find that the scenarios with new physics contributions to the $(C_9^{\rm NP}, C_9')$ or $(C_9^{\rm NP}, C_{10}')$ pair remain the most favored ones. On the other hand, though the competing scenario $(C_9^{\rm NP}, C_{10}^{\rm NP})$ remains attractive, its advantage above the SM reduces significantly due to the tension that emerges between the R_K and R_{K^*} measurements with the new data. The movement of the R_K measurement towards unity would also result in the re-emergence of the one-parameter scenario $C_9^{\rm NP} = -C_9'$.

Keywords: Beyond Standard Model, Heavy Quark Physics

ArXiv ePrint: 1903.09617

https://doi.org/10.1007/JHEP06(2019)089

JHEP06(2019)089

Contents

1 Introduction

The Standard Model (SM) of particle physics cannot be the ultimate theory of fundamental interactions of nature. The necessity for new physics (NP) beyond SM is indicated from multiple directions, such as the neutrino masses, baryon asymmetry in the universe, dark matter, etc. Flavor physics is one of the most incisive probe of such NP, since new particles with masses beyond the reach of current experiments can contribute to low-energy processes through quantum corrections. These NP effects may be measurable at dedicated flavor experiments like LHCb [1] and Belle-II [2], as well as at multipurpose experiments like ATLAS [3] and CMS [4]. Deviations from the SM predictions, observed in the measurements of processes sensitive to such effects, can provide indirect indications of heavy particles or new interactions. These NP effects may be quantified in a model-agnostic way, using the language of effective field theory, by introducing additional operators to the SM effective Hamiltonian governing the relevant processes.

Over the last few years, the rare decays of B mesons, in particular the decays induced by the quark level transition $b \to s\,\ell^+\,\ell^-$ ($\ell = e, \mu$) have already provided some such tantalizing hints of NP.

- The R_K anomaly: the LHCb collaboration, in 2014, reported the measurement of the ratio $R_K \equiv \Gamma(B^+ \to K^+\,\mu^+\,\mu^-)/\Gamma(B^+ \to K^+\,e^+\,e^-)$ in the "low q^2" range ($1.0\,\text{GeV}^2 \leq q^2 \leq 6.0\,\text{GeV}^2$), where q^2 is the invariant mass-squared of the dilepton [5]. This measurement deviates from the SM value of $\simeq 1$ [6, 7] by 2.6 σ, and is an indication of lepton flavor universality (LFU) violation. This measurement was recently updated in Moriond 2019, including the Run-II data and an update of the

JHEP06(2019)089

Run-I analysis. The measurement of R_K from the Run-II data is reported to be $R_K(\text{Run-II}) = 0.928^{+0.089+0.020}_{-0.076-0.017}$, while the combined measurement from both the runs is $R_K(\text{new}) = 0.846^{+0.060+0.016}_{-0.054-0.014}$ [8]. Clearly the central value of R_K is moving towards unity, however the discrepancy with SM has remained $\approx 2.5\sigma$.

- The R_{K^*} anomaly: the LFU violation in $b \to s\,\mu^+\,\mu^-$ sector was further corroborated by the measurement of the related quantity $R_{K^*} \equiv \Gamma(B^0 \to K^{*0}\mu^+\mu^-)/\Gamma(B^0 \to K^{*0}e^+e^-)$ in April 2017. The ratio R_{K^*} was measured in the low-q^2 ($0.045\,\text{GeV}^2 \leq q^2 \leq 1.1\,\text{GeV}^2$), as well as in the central-q^2 ($1.1\,\text{GeV}^2 \leq q^2 \leq 6.0\,\text{GeV}^2$) bin [9]. These measurements differ from the SM predictions of $R_{K^*} \simeq 1$ [6, 7] by $\approx 2.4\sigma$ each. The Belle collaboration has presented their first measurements of R_{K^*} in B^0 decays, and the world's first measurement of R_{K^*} in B^+ decays, in Moriond 2019 [10]. These measurements, in multiple q^2 bins, have comparatively large uncertainties, and hence the anomaly in R_{K^*} still stands at $\approx 2.4\sigma$ level.

- The P_5' anomaly: the values of the angular observable P_5' [11, 12] in $B \to K^*\mu^+\mu^-$ decays, measured by the LHCb [13, 14] as well as ATLAS [15] collaboration in the $4.0\,\text{GeV}^2 \leq q^2 \leq 6.0\,\text{GeV}^2$ bin, differ by $\approx 3.3\sigma$ [16] from their SM prediction [12]. This observable has also been measured by Belle and CMS experiments, albeit in different bins. While the Belle measurement ($4.3\,\text{GeV}^2 \leq q^2 \leq 8.68\,\text{GeV}^2$) differs from the SM by 2.6σ [17], the CMS measurement ($4.3\,\text{GeV}^2 \leq q^2 \leq 6.0\,\text{GeV}^2$) is consistent with the SM to within 1σ [18].

- The B_s^ϕ anomaly: the measured value of the branching ratio of $B_s \to \phi\mu^+\mu^-$ [19, 20] is smaller than the SM prediction [16, 21] by $\approx 3.7\sigma$.

The SM predictions of R_K and R_{K^*} are theoretically clean [6, 7], therefore the deviations of these measurements from the SM are clear indications of NP. On the other hand, the calculations of P_5' and B_s^ϕ involve form factor uncertainties and undetermined power corrections [22–25], so by themselves these two anomalies cannot be considered as unambiguous signals of NP. However, since all these four observables are in the same ($b \to s\ell^+\ell^-$) sector, simultaneous anomalies observed in them should be taken seriously and addressed within the same framework. While the R_K and R_{K^*} anomalies could be due to NP in $b \to s\mu^+\mu^-$ and/or $b \to se^+e^-$ decays [26–29], the discrepancies in P_5' and B_s^ϕ can be attributed to the presence of new physics only in $b \to s\,\mu^+\,\mu^-$. Hence it would be natural to account for all of these anomalies by assuming new physics only in the $b \to s\mu^+\mu^-$ sector, which naturally breaks the LFU. We follow this assumption throughout this work.

We analyze the above four anomalies within the framework of effective field theory, with the aim of gauging the effects of new operators with different Lorentz structures that may contribute to $b \to s\mu\mu$ processes. While the possible Lorentz structures are vector (V), axial vector (A), scalar (S), pseudo-scalar (P), and tensor (T), the last three are heavily constrained from the measurements of $B_s \to \mu\mu$ and $b \to s\gamma$ [30–32]. Hence in our analysis, we consider NP in the form of V and A operators only. Among possible operators, $\mathcal{O}_9 = (\bar{s}\gamma^\mu P_L b)\,(\bar{\mu}\gamma^\mu \mu)$ and $\mathcal{O}_{10} = (\bar{s}\gamma^\mu P_L b)\,(\bar{\mu}\gamma^\mu\gamma^5 \mu)$ already exist in the SM effective Hamiltonian, however their Wilson coefficients (WCs) may be modified due to

JHEP06(2019)089

NP. There are also two chirality-flipped operators, $\mathcal{O}'_9 = (\bar{s}\gamma^\mu P_R b)\,(\bar{\mu}\gamma^\mu \mu)$ and $\mathcal{O}'_{10} = (\bar{s}\gamma^\mu P_R b)\,(\bar{\mu}\gamma^\mu\gamma^5 \mu)$, which do not exist in the SM but may be provided by NP. We represent the WCs of these operators by C_9, C_{10}, C'_9 and C'_{10}, respectively. The NP contribution to C_9 and C_{10} are denoted by $C_9^{\rm NP}$ and $C_{10}^{\rm NP}$, respectively, i.e. $C_9 = C_9^{\rm SM} + C_9^{\rm NP}$ and $C_{10} = C_{10}^{\rm SM} + C_{10}^{\rm NP}$.

After the advent of the R_{K^*} result in 2017, several analyses were performed with an aim of identifying the Lorentz structure of possible NP [27, 33–40]. Most of these analyses showed that these anomalies, except the low-q^2 bin R_{K^*} measurement, may be explained by using a combination of $C_9^{\rm NP}, C_{10}^{\rm NP}, C'_9$, and C'_{10}. The explanation of the R_{K^*} (low-q^2) anomaly would need the introduction of a tensor operator [32], or light Z' mediators [41, 42]. On the other hand, these explanations cannot help in resolving the other anomalies considered in this paper. The resolution of the R_{K^*} (low-q^2) anomaly is therefore taken to be decoupled from that of the others, and we do not dwell on that in this paper.

The most parsimoneous solutions to the anomalies would be the "1D" scenarios, where only one new WC contributes, or the values of two new WCs are related, so that there is only one extra parameter. The scenarios with only-$C_9^{\rm NP}$, $C_9^{\rm NP} = -C_{10}^{\rm NP}$, or $C_9^{\rm NP} = -C'_9$ fit the data much better than the SM [27], though the last one seems to be disfavored since it predicts $R_K \approx 1$ [39]. The above 1D scenarios can indeed be generated in several proposed new physics models that contribute to $b \to s\,\mu^+\mu^-$ at the tree level. For example, Z' models with gauge couplings to leptons can generate the only-$C_9^{\rm NP}$ scenario [43–45]. Some leptoquark models [46–52], and Z' models with loop-induced couplings or with heavy vector-like fermions [53–55], can give rise to $C_9^{\rm NP} = -C_{10}^{\rm NP}$ scenarios. In Z' models with vector-like fermions and $L_\mu - L_\tau$ symmetry, the $C_9^{\rm NP} = -C_9{}'$ scenario may be generated [56].

The "2D" scenarios, where NP contributes to two of the WCs, would be expected to give much better fits to the data than the SM or the 1D fits. The scenarios contributing to the pairs $(C_9^{\rm NP}, C_{10}^{\rm NP}), (C_9^{\rm NP}, C'_9)$ and $(C_9^{\rm NP}, C'_{10})$ have been shown to be able to account for all the above anomalies, except the low-q^2 bin R_{K^*} measurement, to a reasonable extent [27]. Out of these scenarios, the $(C_9^{\rm NP}, C'_9)$ may be generated in Z' models with couplings to leptons through the $L_\mu - L_\tau$ portal [56]. The relative importance of these different 2D scenarios needs to be freshly analyzed in the light of the updated R_K and R_{K^*} results.

In this paper, we analyze all the 2D scenarios, i.e. where NP contributes to two WCs at a time in an uncorrelated manner, with the inclusion of the 2019 Moriond update of the R_K and R_{K^*} data. We perform a global fit to the anomalies as well as to the related data on observables that involve $b \to s\mu\mu$ transitions and would be affected by the same WCs. Since all the observables we consider are CP-conserving, we restrict the WCs to be real. We also consider the fate of the 1D scenarios, which naturally emerge as subsets of the relevant 2D scenarios. We focus on pointing out any changes in the fits to the different scenarios due to the 2019 update. We also interpret these changes in terms of analytic approximations to R_K and R_{K^*} in various scenarios.

The plan of the paper is as follows. In section 2, we discuss the methodology adopted in our analyses. In section 3, we provide the results of our fits and discuss various 2D scenarios and their 1D sub-scenarios. Finally, we summarize and conclude in section 4, with a comparison among different scenarios.

JHEP06(2019)089

2 Methodology

We represent the effective Hamiltonian for the decay $b \to s\mu\mu$ in the presence of new physics V and A operators by

$$\mathcal{H}_{\rm eff}(b \to s\mu\mu) = \mathcal{H}^{\rm SM} + \mathcal{H}^{\rm VA} \,, \tag{2.1}$$

where the SM effective Hamiltonian is

$$\mathcal{H}^{\rm SM} = -\frac{4G_F}{\sqrt{2}\pi} V_{ts}^* V_{tb} \Bigg[\sum_{i=1}^{6} C_i \mathcal{O}_i + C_7 \frac{e}{16\pi^2} [\bar{s}\sigma_{\mu\nu}(m_s P_L + m_b P_R) b] F^{\mu\nu} + C_8 \mathcal{O}_8 + C_9^{\rm SM} \frac{\alpha_{\rm em}}{4\pi} (\bar{s}\gamma^\mu P_L b)(\bar{\mu}\gamma_\mu \mu) + C_{10}^{\rm SM} \frac{\alpha_{\rm em}}{4\pi} (\bar{s}\gamma^\mu P_L b)(\bar{\mu}\gamma_\mu \gamma_5 \mu) \Bigg] \,. \tag{2.2}$$

Here G_F is the Fermi constant and V_{ij} are the Cabibbo-Kobayashi-Maskawa (CKM) matrix elements. The Wilson coefficients C_i of the four-fermi operators $\mathcal{O}_i$ encode the short-distance contributions to the Hamiltonian, where the scale-dependence is implicit, i.e. $C_i \equiv C_i(\mu)$ and $\mathcal{O}_i \equiv \mathcal{O}_i(\mu)$. The operators $\mathcal{O}_i$ $(i = 1, \ldots, 6, 8)$ contribute to these processes through the modifications $C_7(\mu) \to C_7^{\rm eff}(\mu, q^2)$ and $C_9(\mu) \to C_9^{\rm eff}(\mu, q^2)$, where q^2 is the invariant mass-squared of the final state muon pair. The NP effective Hamiltonian is

$$\mathcal{H}^{\rm VA} = -\frac{\alpha_{\rm em} G_F}{\sqrt{2}\pi} V_{ts}^* V_{tb} \Big[C_9^{\rm NP} (\bar{s}\gamma^\mu P_L b)(\bar{\mu}\gamma_\mu \mu) + C_{10}^{\rm NP} (\bar{s}\gamma^\mu P_L b)(\bar{\mu}\gamma_\mu \gamma_5 \mu) + C_9' (\bar{s}\gamma^\mu P_R b)(\bar{\mu}\gamma_\mu \mu) + C_{10}' (\bar{s}\gamma^\mu P_R b)(\bar{\mu}\gamma_\mu \gamma_5 \mu) \Big] . \tag{2.3}$$

The NP effects are thus encoded in the Wilson coefficients $C_9^{\rm NP}, C_{10}^{\rm NP}, C_9'$ and C_{10}'.

While NP can in principle contribute to all the above four WCs, we focus on those scenarios where only two of these coefficients are nonzero. While this restriction is somewhat arbitrary at this stage, it is possible that symmetries of the NP at high scales can naturally make some of these coefficients vanish. The scenarios we consider may provide clearer insights on the role of NP Lorentz structures, due to the smaller number of parameters involved. We consider all six possible pairs of these coefficients, viz. $(C_9^{\rm NP}, C_{10}^{\rm NP})$, $(C_9^{\rm NP}, C_9')$, $(C_9^{\rm NP}, C_{10}')$, $(C_{10}^{\rm NP}, C_9')$, $(C_{10}^{\rm NP}, C_{10}')$ and (C_9', C_{10}'). This analysis is also naturally applicable to the scenarios where only one of these coefficients is nonzero, or the two are linearly related, as considered in [57–59].

For each of these pairs of WCs, we perform a global fit to the observables that would be influenced by these WCs. Apart from the four observables that have indicated anomalies, viz. R_K, R_{K^*}, P_5', B_s^ϕ, we also include the constraints from (i) the branching ratio of $B_s \to \mu\mu$ [60–62], (ii) the differential branching ratios of $B^0 \to K^{*0}\mu^+\mu^-$ [63–66], $B^+ \to K^{*+}\mu^+\mu^-$, $B^0 \to K^0\mu^+\mu^-$, $B^+ \longrightarrow K^+\mu^+\mu^-$ [64, 67], and $B \to X_s\mu^+\mu^-$ [68] in several q^2 bins, (iii) angular observables in $B^0 \to K^{*0}\mu^+\mu^-$ [14, 15, 18, 64, 66] and $B_s^0 \to \phi\mu^+\mu^-$ [20] in several q^2 bins. For global fits with the new data, we include the updated measurement of R_K [8] and the new measurements of R_{K^*} by the Belle collaboration (the bins $0.045\,\text{GeV}^2 < q^2 < 1.1\,\text{GeV}^2$, $1.1\,\text{GeV}^2 < q^2 < 6.0\,\text{GeV}^2$, and $15.0\,\text{GeV}^2 < q^2 < 19.0\,\text{GeV}^2$), for B^0 as well as B^+ decays [10].

JHEP06(2019)089

Note that all these observables are CP-conserving, as a result we do not expect to be sensitive to the complex nature of the new WCs. We therefore take $C_9^{\rm NP}, C_{10}^{\rm NP}, C_9'$ and C_{10}' to be real for the sake of this article. We perform a two-dimensional (2D) χ^2 fit using the CERN minimization code `MINUIT` [69]. The χ^2 function is defined as

$$\chi^2(C_i, C_j) = \left[\mathcal{O}_{\rm th}(C_i, C_j) - \mathcal{O}_{\rm exp}\right]^T \mathcal{C}^{-1} \left[\mathcal{O}_{\rm th}(C_i, C_j) - \mathcal{O}_{\rm exp}\right]. \tag{2.4}$$

Here $\mathcal{O}_{\rm th}(C_i, C_j)$ are the theoretical predictions of the N=116 (122) observables before (after) the Moriond 2019 update used in the fit, while $\mathcal{O}_{\rm exp}$ are the experimental measurements. The $N \times N$ total covariance matrix $\mathcal{C}$ is obtained by adding the individual theoretical and experimental covariance matrices. The values of $\mathcal{O}_{\rm th}(C_i, C_j)$ and the theoretical covariance matrix are calculated using `flavio` [70]. The correlations among $\mathcal{O}_{\rm exp}$ are included for the angular observables in $B \to K^{(*)}\mu^+\mu^-$ [14] and $B_s \to \phi\mu^+\mu^-$ [20]. For the branching ratio of $B_s \to \mu\mu$, we use the combined fit to $B_s \to \mu\mu$ and $B^0 \to \mu\mu$ measurements [60–62], obtained by taking $B^0 \to \mu\mu$ to be SM-like [72]. For the other observables, we add the statistical and systematic errors in quadrature. Wherever the errors are asymmetric, we use the conservative approach of using the larger error on both sides of the central value.

We denote the value of χ^2 in the SM by $\chi^2_{\rm SM}$, and the best-fit value in the presence of NP by $\chi^2_{\rm bf}$. Clearly the addition of two degrees of freedom provided by the two new WCs decreases the χ^2, and hence $\chi^2_{\rm SM} > \chi^2_{\rm bf}$. We define $\Delta\chi^2 \equiv \chi^2_{\rm SM} - \chi^2_{\rm bf}$ for each pair of WCs, which would enable us to quantify the extent to which a particular combination of WCs is able to provide a better fit to the data. For convenience of notation, we denote the value of $\Delta\chi^2$ before (after) the 2019 update as $\Delta\chi^2_{\rm old}$ ($\Delta\chi^2_{\rm new}$).

3 Results and discussions

We present the results of our 2D fits in the form of contour plots in the parameter space of the two relevant WCs, as shown in figure 1. The six plots correspond to the six scenarios with nonzero NP contributions to $(C_9^{\rm NP}, C_{10}^{\rm NP})$, $(C_9^{\rm NP}, C_9')$, $(C_9^{\rm NP}, C_{10}')$, $(C_{10}^{\rm NP}, C_9')$, $(C_{10}^{\rm NP}, C_{10}')$ and (C_9', C_{10}'), respectively. In all plots, SM corresponds to the point $(0, 0)$.

In the figure, we show the 1σ regions allowed from the measurements of (i) the ratio R_{K^*} (central bin: $1.0\,{\rm GeV}^2 < q^2 < 6.0\,{\rm GeV}^2$), (ii) the average of the angular observable P_5' ($4.0\,{\rm GeV}^2 < q^2 < 6.0\,{\rm GeV}^2$) from the ATLAS and LHCb experiments [16], and (iii) the branching ratio $\mathcal{B}(B_s \to \phi\,\mu^+\mu^-)$, with bands of blue, pink, and green color, respectively. The 1σ allowed region of R_K from the 2014 data [5] and the updated 2019 data [8] are shown by light and dark yellow bands, respectively. The overlaps (or lack of them) of these bands contain information about the consistency (or tension) among different anomalies. Note that none of these scenarios is able to account for the measured value of R_{K^*} in the low-q^2 bin within 2σ. So the band corresponding to this measurement is not shown in the plots, though it contributes to the global fit. Also, the CMS results on P_5' [66] are not shown in the bands since they correspond to a different q^2-range. The new R_{K^*} result from Belle [10] are also not shown, since they currently have large uncertainties. These results are, however, included in the global fit.

JHEP06(2019)089

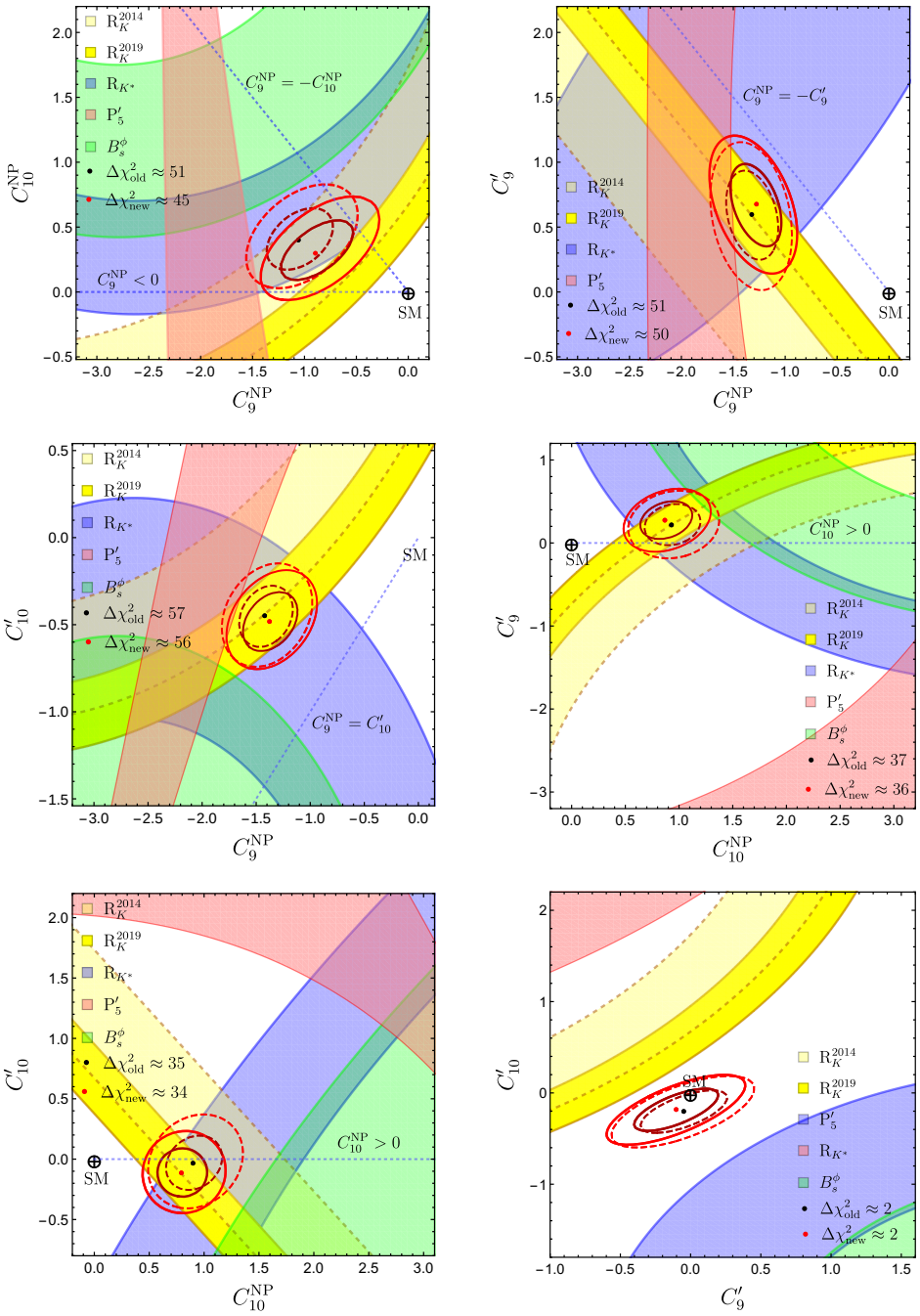

Figure 1. The 1σ allowed bands for R_K ($1.0\,\text{GeV}^2 < q^2 < 6.0\,\text{GeV}^2$) before and after 2019 update, R_{K^*} in the central bin ($1.0\,\text{GeV}^2 < q^2 < 6.0\,\text{GeV}^2$), P_5' ($4.0\,\text{GeV}^2 < q^2 < 6.0\,\text{GeV}^2$) from ATLAS and LHCb, and $B_s^\phi \equiv \mathcal{B}(B_s \to \phi\mu^+\mu^-)$ in the range ($1.0\,\text{GeV}^2 < q^2 < 6.0\,\text{GeV}^2$), for the six 2D scenarios. The 1σ and 2σ allowed regions from the global fit using data before (after) the 2019 R_K update are shown by dashed (solid) contours. Specific 1D sub-scenarios that give a good fit to the data are also shown.

JHEP06(2019)089

Wilson Coefficient(s)	Before `Moriond 2019`		After `Moriond 2019`	
	Best fit values(s)	$\Delta\chi^2_{\rm old}$	Best fit values(s)	$\Delta\chi^2_{\rm new}$
$C_i = 0$ (SM)	—	0	—	0
1D Scenarios:				
$C_9^{\rm NP}$	-1.22 ± 0.18	42.7	-1.09 ± 0.18	39.0
$C_{10}^{\rm NP}$	$+0.89 \pm 0.17$	34.2	$+0.79 \pm 0.15$	32.3
$C_9^{\prime}$	$+0.17 \pm 0.16$	1.04	$+0.09 \pm 0.15$	0.40
$C_{10}^{\prime}$	-0.22 ± 0.12	3.06	-0.16 ± 0.11	1.92
$C_9^{\rm NP} = C_{10}^{\rm NP}$	$+0.20 \pm 0.18$	1.34	$+0.20 \pm 0.17$	1.40
$C_9^{\rm NP} = -C_{10}^{\rm NP}$	-0.65 ± 0.10	46.5	-0.53 ± 0.09	41.0
$C_9^{\prime} = C_{10}^{\prime}$	-0.20 ± 0.16	1.62	-0.19 ± 0.16	1.51
$C_9^{\prime} = -C_{10}^{\prime}$	$+0.12 \pm 0.08$	2.49	$+0.08 \pm 0.07$	1.32
$C_9^{\rm NP} = C_9^{\prime}$	-0.44 ± 0.14	11.8	-0.35 ± 0.12	10.8
$C_9^{\rm NP} = -C_9^{\prime}$	-1.12 ± 0.17	41.9	-1.12 ± 0.17	41.4
$C_{10}^{\rm NP} = C_{10}^{\prime}$	$+0.37 \pm 0.13$	9.59	$+0.29 \pm 0.11$	8.99
$C_{10}^{\rm NP} = -C_{10}^{\prime}$	$+0.43 \pm 0.10$	22.3	$+0.42 \pm 0.10$	22.3
$C_9^{\rm NP} = C_{10}^{\prime}$	-0.68 ± 0.12	33.5	-0.66 ± 0.11	32.3
$C_9^{\rm NP} = -C_{10}^{\prime}$	-0.18 ± 0.09	3.79	-0.17 ± 0.08	4.24
$C_{10}^{\rm NP} = C_9^{\prime}$	$+0.59 \pm 0.12$	27.3	$+0.58 \pm 0.12$	27.0
$C_{10}^{\rm NP} = -C_9^{\prime}$	$+0.39 \pm 0.11$	13.5	$+0.32 \pm 0.09$	12.6
2D Scenarios:				
$(C_9^{\rm NP}, C_{10}^{\rm NP})$	$(-1.06, +0.40)$	51.4	$(-0.90, +0.30)$	44.7
$(C_9^{\prime}, C_{10}^{\prime})$	$(-0.05, -0.20)$	2.26	$(-0.10, -0.19)$	1.57
$(C_9^{\rm NP}, C_9^{\prime})$	$(-1.32, +0.60)$	51.1	$(-1.28, +0.68)$	50.3
$(C_9^{\rm NP}, C_{10}^{\prime})$	$(-1.42, -0.45)$	57.4	$(-1.38, -0.48)$	56.5
$(C_{10}^{\rm NP}, C_9^{\prime})$	$(+0.93, +0.22)$	36.7	$(+0.87, +0.27)$	36.2
$(C_{10}^{\rm NP}, C_{10}^{\prime})$	$(+0.90, -0.03)$	35.1	$(+0.79, -0.11)$	33.7

Table 1. Best fit values of new WCs in various 1D and 2D scenarios. The improvement over SM is quantified by $\Delta\chi^2 \equiv \chi^2_{\rm SM} - \chi^2_{\rm bf}$. For 1D scenarios, the 1σ allowed ranges of the relevant WC are also provided. With the 2019 Moriond update, the value of $\chi^2_{\rm SM}$ goes from 157 to 156.

Superimposed on the above bands are the 1σ and 2σ contours, shown in brown and red, respectively, corresponding to the global fit to all 116 (122) observables, before (after) the Moriond 2019 update. The contours corresponding to the data before (after) the update have dashed (solid) boundaries. A comparison of these two sets of contours gives us an indication of how the preferred parameter space in the particular NP scenario has changed due to the 2019 update. The superposition of these contours on the 1σ bands of key individual measurements above allows us to check whether the best-fit region is indeed able to account for all the anomalies.

JHEP06(2019)089

Some of the plots also indicate the lines corresponding to selected scenarios with linear relations between the two WCs which give good fits to the data. While the viability of these 1D sub-scenarios may be judged qualitatively from the figures, table 1 lists the best-fit values of parameters, along with the $\Delta\chi^2_{\rm old}$, $\Delta\chi^2_{\rm new}$, and 1σ allowed regions for them.

Below we list some important observations that may be made for the six scenarios. Since the measurements of R_K and R_{K^*} are theoretically clean, and are expected to dominate the fits, we also try to understand the impact of new R_K and R_{K^*} measurements by using analytic approximations for R_K and R_{K^*} (central-q^2) in the presence of the corresponding NP. Henceforth in this section, we shall refer to R_{K^*} (central-q^2) simply as R_{K^*} for the sake of brevity.

3.1 The $(C_9^{\rm NP}, C_{10}^{\rm NP})$ scenario

This scenario improves the global fit significantly as compared to the SM, however $\Delta\chi^2_{\rm new} \approx 45$ has decreased substantially from its older value of $\Delta\chi^2_{\rm old} \approx 51$. This is partly an effect of the new R_K measurement having moved closer to the SM prediction. The new measurements have also increased the tension of the global best fit with all the four individual anomalies marginally. This scenario still stands as one of the favored ones to account for these anomalies. The 1D sub-scenarios $C_9^{\rm NP} = -C_{10}^{\rm NP}$ and $C_{10}^{\rm NP} = 0$ also continue to improve the global fit, however the extent of improvement has reduced for $C_9^{\rm NP} = -C_{10}^{\rm NP}$ ($C_{10}^{\rm NP} = 0$) to $\Delta\chi^2_{\rm new} \approx 41$ (39) with the new data, compared to $\Delta\chi^2_{\rm old} \approx 46$ (43) from earlier.

The relatively sharp decrease (compared to the other scenarios) in the value of $\Delta\chi^2$ after the Moriond 2019 update may be understood from the approximate functional forms [71]

$$R_K = R_{K^*} \approx 1 + 0.24\,(C_9^{\rm NP} - C_{10}^{\rm NP})\,. \tag{3.1}$$

It can be seen that the values of R_K and R_{K^*} are forced to be approximately equal in this scenario. While this was indeed the case before the update, after the update one has $R_K \approx 0.85$ and $R_{K^*} \approx 0.69$. Thus, a tension has emerged in the measurements of these two quantities, thereby decreasing the overall goodness of fit.

3.2 The $(C_9^{\rm NP}, C_9')$ scenario

This scenario already provided a slightly better fit to the data than the $(C_9^{\rm NP}, C_{10}^{\rm NP})$ scenario, even before the 2019 update. With the update, $\Delta\chi^2_{\rm old} \approx 51$ for this scenario has stayed almost the same at $\Delta\chi^2_{\rm new} \approx 50$, indicating that it is still able to explain most of the data much better than the SM. Indeed, the fit is still consistent with R_{K^*} and P_5', while its agreement with R_K has improved with the new data. The 1D sub-scenario $C_9^{\rm NP} = -C_9'$ also has continued to provide a good fit to the data ($\Delta\chi^2_{\rm new} \approx 41$), however earlier it was considered to be disfavored as it predicted $R_K \approx 1$ [39]. The updated data, however, has moved R_K closer to unity. If this trend continues, this scenario could re-emerge as a favored NP solution.

In the $(C_9^{\rm NP}, C_9')$ scenario, the choices for $C_9^{\rm NP}$ and C_9' can allow R_K and R_{K^*} to vary independently:

$$R_K \approx 1 + 0.24\,(C_9^{\rm NP} + C_9')\ ,\ R_{K^*} \approx 1 + 0.24\,C_9^{\rm NP} - 0.17 C_9'\,. \tag{3.2}$$

No significant tension is therefore created because of the updated value of R_K. The increase in the central value of R_K after the update has only shifted the best fit point in the $(C_9^{\rm NP}, C_9')$ plane to higher values of $C_9^{\rm NP}$ and C_9'. More importantly, the increase in the R_K measurement has directly decreased the value of the combination $C_9^{\rm NP} + C_9'$, making the 1D sub-scenario $C_9^{\rm NP} = -C_9'$ more viable.

3.3 The $(C_9^{\rm NP}, C_{10}')$ scenario

This scenario was the one with the largest $\Delta\chi^2_{\rm old} \approx 57$ among all the 2D global fits before the update, and stays so ($\Delta\chi^2_{\rm new} \approx 56$) even with the update. It can accommodate R_K and R_{K^*} anomalies within 1σ, and is quite close to the 1σ allowed regions for P_5' and B_s^ϕ. Note that the possible 1D sub-scenarios $C_9^{\rm NP} = 0$ or $C_9^{\rm NP} = -C_{10}'$ do not improve the SM fit significantly, while $C_9^{\rm NP} = C_{10}'$ ($C_{10}' = 0$) improves it by $\Delta\chi^2_{\rm new} \approx 32\,(39)$.

As far as the dependence of R_K and R_{K^*} on the NP parameters is concerned, this scenario is similar to the previous one:

$$R_K \approx 1 + 0.24\,(C_9^{\rm NP} - C_{10}')\ ,\ R_{K^*} \approx 1 + 0.24\,C_9^{\rm NP} + 0.17 C_{10}'\ . \tag{3.3}$$

While both these scenarios perform equally well in accounting for R_K, R_{K^*}, and P_5', the $(C_9^{\rm NP}, C_{10}')$ scenario can accommodate B_s^ϕ values closer to its measurement, and hence has a slightly better $\Delta\chi^2$ than $(C_9^{\rm NP}, C_9')$. The updated R_K measurement shifts the best fit point to higher $C_9^{\rm NP}$ and lower C_{10}'.

3.4 The $(C_{10}^{\rm NP}, C_9')$ scenario

This scenario offers a moderate improvement over the SM, with $\Delta\chi^2_{\rm new} \approx 36$. The best fit for this scenario continues to be able to account for the R_K and R_{K^*} anomalies to within 1σ, however it cannot explain P_5' even within 2σ. The 1D sub-scenarios $C_{10}^{\rm NP} = C_9'$ ($\Delta\chi^2_{\rm new} \approx 27$) and $C_9' = 0$ ($\Delta\chi^2_{\rm new} \approx 32$) offer some improvement over the SM, however $C_{10}^{\rm NP} = -C_9'$ can only allow $\Delta\chi^2_{\rm new} \approx 12$.

The approximate functional forms of R_K and R_{K^*} in this scenario are

$$R_K \approx 1 + 0.24\,(-C_{10}^{\rm NP} + C_9')\ ,\ R_{K^*} \approx 1 - 0.24\,C_{10}^{\rm NP} - 0.17 C_9'\ . \tag{3.4}$$

Since C_9' contributes to R_K and R_{K^*} with opposite signs, in order to have both R_K and R_{K^*} values less than unity, one would need a large value of $C_{10}^{\rm NP}$. However, such a large value of $C_{10}^{\rm NP}$ is disfavoured by $B_s \to \mu^+\mu^-$ measurement, which is close to its SM prediction. As a result, the improvement above SM is not significant in this scenario.

3.5 The $(C_{10}^{\rm NP}, C_{10}')$ scenario

This scenario offers a moderate improvement over the SM, with $\Delta\chi^2_{\rm new} \approx 34$. The best fit for this scenario continues to be able to account for the R_K and R_{K^*} anomalies to within 1σ, however it cannot explain P_5' even within 2σ. The 1D sub-scenarios, $C_{10}^{\rm NP} = -C_{10}'$ and $C_{10}' = 0$ offer some improvement ($\Delta\chi^2_{\rm new} \approx 22$ and $\Delta\chi^2_{\rm new} \approx 32$, respectively) over the SM, however $C_{10}^{\rm NP} = C_{10}'$ can only allow $\Delta\chi^2_{\rm new} \approx 9$.

JHEP06(2019)089

The reason for only a moderate improvement in the goodness of fit over the SM is similar to the one in the previous scenario. Here,

$$R_K \approx 1 + 0.24\,(-C_{10}^{\rm NP} - C'_{10})\ ,\ R_{K^*} \approx 1 - 0.24\,C_{10}^{\rm NP} + 0.17 C'_{10}\ . \tag{3.5}$$

Thus C'_{10} contributes to R_K and R_{K^*} with opposite signs, forcing $C_{10}^{\rm NP}$ to have unreasonably large values.

3.6 The (C'_9, C'_{10}) scenario

This scenario is not able to offer any significant improvement over the SM: both $\Delta\chi^2_{\rm old}$ and $\Delta\chi^2_{\rm new}$ are less than 3. As can be seen from the figure, the pairs of measurements (R_K, P'_5) and (R_{K^*}, B_s^ϕ) pull the best fit point in almost opposite directions, thus keeping it close to the SM, without offering any solution to the anomalies. These opposite pulls are mainly the result of R_K and R_{K^*} measurements. We have

$$R_K \approx 1 + 0.24\,(C'_9 - C'_{10})\ ,\ R_{K^*} \approx 1 + 0.17\,(-C'_9 + C'_{10})\ . \tag{3.6}$$

In the presence of only these two new WCs, the values of R_K and R_{K^*} are forced in opposite directions from unity. As long as the measured values of R_K and R_{K^*} are both less than unity, the allowed values of C'_9 and C'_{10} will stay small and cannot contribute to resolving both the anomalies simultaneously. The global fit will therefore stay poor.

4 Summary and conclusions

In this paper, we have explored whether pairs of new vector or axial vector effective operators would allow us to explain the anomalies observed in $b \to s$ decays, namely R_K, R_{K^*}, P'_5, and B_s^ϕ. We have analyzed all the six pairwise combinations of the NP Wilson coefficients $C_9^{\rm NP}, C_{10}^{\rm NP}, C'_9, C'_{10}$ that may contribute to the resolutions of these anomalies. We have performed global fits to data available before and after the Moriond 2019 update of R_K and R_{K^*}, in order to obtain the favored values of the relevant WCs in these six scenarios. Our 2D global fits lead to the following observations:

- The two scenarios $(C_9^{\rm NP}, C'_9)$ and $(C_9^{\rm NP}, C'_{10})$ continue to offer significantly better fits to the data as compared to the SM ($\Delta\chi^2_{\rm new} > 50$), even with the 2019 update to the data. Both of these best fits can account for R_K, R_{K^*} anomalies within 1σ, and P'_5, B_s^ϕ anomalies within 2σ.

- The scenario $(C_9^{\rm NP}, C_{10}^{\rm NP})$, which used to give a significantly better fit ($\Delta\chi^2_{\rm old} \approx 51$) than the SM before the 2019 update, cannot offer as good an improvement ($\Delta\chi^2_{\rm new} \approx 45$) over the SM after the update. Indeed it is the only 2D scenario whose $\Delta\chi^2$ has undergone such a sharp decrease after the update, compared to the other ones. The scenario is still viable, though the tensions with individual experiments have increased with the update. The root cause of this may be traced to the approximately identical functional dependence of R_K and R_{K^*} to the two WCs, $C_9^{\rm NP}$ and $C_{10}^{\rm NP}$, in this scenario.

JHEP06(2019)089

- The scenarios $(C_{10}^{\rm NP}, C_9')$ and $(C_{10}^{\rm NP}, C_{10}')$ continue to offer only moderate improvements ($\Delta\chi^2_{\rm new} \approx 35$) over the SM. The worst scenario for explaining the anomalies turns out to be (C_9', C_{10}'). The best fit for this scenario is very close to the SM, and does not help in the simultaneous explanation of the anomalies.

Many features of the above global fits, and the changes in these fits after the R_K and R_{K^*} update, may be understood in terms of the effect of new WCs on R_K and R_{K^*} using analytic approximations. Note that the anomaly in the low-q^2 bin of R_{K^*} cannot be explained by any of these 2D fits, as has been pointed out earlier.

These 2D fits also allow us to explore their 1D sub-scenarios where only one new WC is nonzero, or where the two new WCs are linearly related. Such scenarios may be interesting not only from the point of view of smaller number of parameters, but also because such relations may prevent unwelcome effective operators from getting generated. The following 1D sub-scenarios offer significant improvements above the SM:

- The $C_9^{\rm NP} = -C_9'$ scenario can give $\Delta\chi^2_{\rm new} \approx 41$. While this was still the case before the update, it was not considered to be a favored scenario since it predicted $R_K \approx 1$, in conflict with the older data. The update has moved R_K in the direction of unity, and has made this scenario more attractive.

- The scenarios $C_9^{\rm NP} = -C_{10}^{\rm NP}$ ($\Delta\chi^2_{\rm new} \approx 41$) and $C_9^{\rm NP} = C_{10}'$ ($\Delta\chi^2_{\rm new} \approx 32$) provide moderate improvements over the SM.

In our analysis, we have taken the data-driven approach and considered the addition of only a single, or a couple of, NP operators. While these would appear to be the most economical solutions in the language of effective field theory, they may not be always so from the point of view of constructing a high scale theory. While reducing the high scale theory to a low scale effective theory, the desired new effective operator(s) may be necessarily accompanied by other additional effective operators with different Lorentz structures. Putting the coefficients of these effective operators to zero is a possible way out, however the stability of such a scenario needs to be guaranteed by a symmetry at the high scale, or the scenario would involve some fine tuning of parameters. Here we take the approach that having a good fit in a 2D scenario guarantees an equally good (if not better) fit in the space with more than two NP parameters. The favored scenarios that have emerged with the updated data could help in narrowing down possible NP models and guiding constructions of models beyond the current paradigm.

Acknowledgments

We would like to thank Diptimoy Ghosh, Jacky Kumar and Gagan Mohanty for useful discussions. The work of DK is partially supported by the National Science Centre (Poland) under the research grant No. 2017/26/E/ST2/00470.

JHEP06(2019)089

References

[1] LHCb collaboration, *The LHCb detector at the LHC*, 2008 *JINST* **3** S08005 [INSPIRE].

[2] BELLE-II collaboration, *Belle II technical design report*, arXiv:1011.0352 [INSPIRE].

[3] ATLAS collaboration, *The ATLAS experiment at the CERN Large Hadron Collider*, 2008 *JINST* **3** S08003 [INSPIRE].

[4] CMS collaboration, *The CMS experiment at the CERN LHC*, 2008 *JINST* **3** S08004 [INSPIRE].

[5] LHCb collaboration, *Test of lepton universality using $B^+ \to K^+\ell^+\ell^-$ decays*, *Phys. Rev. Lett.* **113** (2014) 151601 [arXiv:1406.6482] [INSPIRE].

[6] G. Hiller and F. Krüger, *More model-independent analysis of $b \to s$ processes*, *Phys. Rev.* **D 69** (2004) 074020 [hep-ph/0310219] [INSPIRE].

[7] M. Bordone, G. Isidori and A. Pattori, *On the standard model predictions for R_K and R_{K^*}*, *Eur. Phys. J.* **C 76** (2016) 440 [arXiv:1605.07633] [INSPIRE].

[8] LHCb collaboration, *Search for lepton-universality violation in $B^+ \to K^+\ell^+\ell^-$ decays*, *Phys. Rev. Lett.* **122** (2019) 191801 [arXiv:1903.09252] [INSPIRE].

[9] LHCb collaboration, *Test of lepton universality with $B^0 \to K^{*0}\ell^+\ell^-$ decays*, *JHEP* **08** (2017) 055 [arXiv:1705.05802] [INSPIRE].

[10] BELLE collaboration, *Test of lepton flavor universality in $B \to K^*\ell^+\ell^-$ decays at Belle*, arXiv:1904.02440 [INSPIRE].

[11] S. Descotes-Genon, J. Matias, M. Ramon and J. Virto, *Implications from clean observables for the binned analysis of $B \to K*\mu^+\mu^-$ at large recoil*, *JHEP* **01** (2013) 048 [arXiv:1207.2753] [INSPIRE].

[12] S. Descotes-Genon, T. Hurth, J. Matias and J. Virto, *Optimizing the basis of $B \to K^*ll$ observables in the full kinematic range*, *JHEP* **05** (2013) 137 [arXiv:1303.5794] [INSPIRE].

[13] LHCb collaboration, *Measurement of form-factor-independent observables in the decay $B^0 \to K^{*0}\mu^+\mu^-$*, *Phys. Rev. Lett.* **111** (2013) 191801 [arXiv:1308.1707] [INSPIRE].

[14] LHCb collaboration, *Angular analysis of the $B^0 \to K^{*0}\mu^+\mu^-$ decay using 3 fb^{-1} of integrated luminosity*, *JHEP* **02** (2016) 104 [arXiv:1512.04442] [INSPIRE].

[15] ATLAS collaboration, *Angular analysis of $B_d^0 \to K^*\mu^+\mu^-$ decays in pp collisions at $\sqrt{s} = 8$ TeV with the ATLAS detector*, *JHEP* **10** (2018) 047 [arXiv:1805.04000] [INSPIRE].

[16] J. Aebischer, J. Kumar, P. Stangl and D.M. Straub, *A global likelihood for precision constraints and flavour anomalies*, arXiv:1810.07698 [INSPIRE].

[17] BELLE collaboration, *Angular analysis of $B^0 \to K^*(892)^0\ell^+\ell^-$*, arXiv:1604.04042 [INSPIRE].

[18] CMS collaboration, *Measurement of the P_1 and P_5' angular parameters of the decay $B^0 \to K^{*0}\mu^+\mu^-$ in proton-proton collisions at $\sqrt{s} = 8$ TeV*, CMS-PAS-BPH-15-008 (2015).

[19] LHCb collaboration, *Differential branching fraction and angular analysis of the decay $B_s^0 \to \phi\mu^+\mu^-$*, *JHEP* **07** (2013) 084 [arXiv:1305.2168] [INSPIRE].

[20] LHCb collaboration, *Angular analysis and differential branching fraction of the decay $B_s^0 \to \phi\mu^+\mu^-$*, *JHEP* **09** (2015) 179 [arXiv:1506.08777] [INSPIRE].

JHEP06(2019)089

[21] A. Bharucha, D.M. Straub and R. Zwicky, *$B \to V\ell^+\ell^-$ in the standard model from light-cone sum rules*, *JHEP* **08** (2016) 098 [arXiv:1503.05534] [INSPIRE].

[22] A. Khodjamirian, T. Mannel, A.A. Pivovarov and Y.M. Wang, *Charm-loop effect in $B \to K^{(*)}\ell^+\ell^-$ and $B \to K^*\gamma$*, *JHEP* **09** (2010) 089 [arXiv:1006.4945] [INSPIRE].

[23] C. Bobeth, M. Chrzaszcz, D. van Dyk and J. Virto, *Long-distance effects in $B \to K^*\ell\ell$ from analyticity*, *Eur. Phys. J.* **C 78** (2018) 451 [arXiv:1707.07305] [INSPIRE].

[24] T. Blake et al., *An empirical model to determine the hadronic resonance contributions to $\overline{B}^0 \to \overline{K}^{*0}\mu^+\mu^-$ transitions*, *Eur. Phys. J.* **C 78** (2018) 453 [arXiv:1709.03921] [INSPIRE].

[25] A. Arbey, T. Hurth, F. Mahmoudi and S. Neshatpour, *Hadronic and new physics contributions to $b \to s$ transitions*, *Phys. Rev.* **D 98** (2018) 095027 [arXiv:1806.02791] [INSPIRE].

[26] D. Bhatia, S. Chakraborty and A. Dighe, *Neutrino mixing and R_K anomaly in $\mathrm{U}(1)_X$ models: a bottom-up approach*, *JHEP* **03** (2017) 117 [arXiv:1701.05825] [INSPIRE].

[27] B. Capdevila et al., *Patterns of new physics in $b \to s\ell^+\ell^-$ transitions in the light of recent data*, *JHEP* **01** (2018) 093 [arXiv:1704.05340] [INSPIRE].

[28] J. Kumar and D. London, *New physics in $b \to se^+e^-$?*, *Phys. Rev.* **D 99** (2019) 073008 [arXiv:1901.04516] [INSPIRE].

[29] G. D'Ambrosio, A.M. Iyer, F. Piccinini and A.D. Polosa, *Confronting B anomalies with atomic physics*, arXiv:1902.00893 [INSPIRE].

[30] A.K. Alok et al., *New physics in $b \to s\mu^+\mu^-$: CP-conserving observables*, *JHEP* **11** (2011) 121 [arXiv:1008.2367] [INSPIRE].

[31] A.K. Alok et al., *New physics in $b \to s\mu^+\mu^-$: CP-violating observables*, *JHEP* **11** (2011) 122 [arXiv:1103.5344] [INSPIRE].

[32] D. Bardhan, P. Byakti and D. Ghosh, *Role of tensor operators in R_K and R_{K^*}*, *Phys. Lett.* **B 773** (2017) 505 [arXiv:1705.09305] [INSPIRE].

[33] W. Altmannshofer, P. Stangl and D.M. Straub, *Interpreting hints for lepton flavor universality violation*, *Phys. Rev.* **D 96** (2017) 055008 [arXiv:1704.05435] [INSPIRE].

[34] G. D'Amico et al., *Flavour anomalies after the R_{K^*} measurement*, *JHEP* **09** (2017) 010 [arXiv:1704.05438] [INSPIRE].

[35] G. Hiller and I. Nisandzic, *R_K and R_{K^*} beyond the standard model*, *Phys. Rev.* **D 96** (2017) 035003 [arXiv:1704.05444] [INSPIRE].

[36] L.-S. Geng et al., *Towards the discovery of new physics with lepton-universality ratios of $b \to s\ell\ell$ decays*, *Phys. Rev.* **D 96** (2017) 093006 [arXiv:1704.05446] [INSPIRE].

[37] M. Ciuchini et al., *On flavourful easter eggs for new physics hunger and lepton flavour universality violation*, *Eur. Phys. J.* **C 77** (2017) 688 [arXiv:1704.05447] [INSPIRE].

[38] A. Celis, J. Fuentes-Martin, A. Vicente and J. Virto, *Gauge-invariant implications of the LHCb measurements on lepton-flavor nonuniversality*, *Phys. Rev.* **D 96** (2017) 035026 [arXiv:1704.05672] [INSPIRE].

[39] A.K. Alok et al., *New Physics in $b \to s\mu^+\mu^-$ after the measurement of R_{K^*}*, *Phys. Rev.* **D 96** (2017) 095009 [arXiv:1704.07397] [INSPIRE].

JHEP06(2019)089

[40] A.K. Alok et al., *New physics in $b \to s\mu^+\mu^-$: distinguishing models through CP-violating effects*, *Phys. Rev.* **D 96** (2017) 015034 [arXiv:1703.09247] [INSPIRE].

[41] A. Datta, J. Kumar, J. Liao and D. Marfatia, *New light mediators for the R_K and R_{K^*} puzzles*, *Phys. Rev.* **D 97** (2018) 115038 [arXiv:1705.08423] [INSPIRE].

[42] W. Altmannshofer et al., *Light resonances and the low-q^2 bin of R_{K^*}*, *JHEP* **03** (2018) 188 [arXiv:1711.07494] [INSPIRE].

[43] A. Crivellin, G. D'Ambrosio and J. Heeck, *Addressing the LHC flavor anomalies with horizontal gauge symmetries*, *Phys. Rev.* **D 91** (2015) 075006 [arXiv:1503.03477] [INSPIRE].

[44] B. Allanach, F.S. Queiroz, A. Strumia and S. Sun, *Z' models for the LHCb and $g-2$ muon anomalies*, *Phys. Rev.* **D 93** (2016) 055045 [*Erratum ibid.* **D 95** (2017) 119902] [arXiv:1511.07447] [INSPIRE].

[45] W. Altmannshofer, S. Gori, S. Profumo and F.S. Queiroz, *Explaining dark matter and B decay anomalies with an $L_\mu - L_\tau$ model*, *JHEP* **12** (2016) 106 [arXiv:1609.04026] [INSPIRE].

[46] B. Gripaios, M. Nardecchia and S.A. Renner, *Composite leptoquarks and anomalies in B-meson decays*, *JHEP* **05** (2015) 006 [arXiv:1412.1791] [INSPIRE].

[47] S. Fajfer and N. Košnik, *Vector leptoquark resolution of R_K and $R_{D^{(*)}}$ puzzles*, *Phys. Lett.* **B 755** (2016) 270 [arXiv:1511.06024] [INSPIRE].

[48] I. de Medeiros Varzielas and G. Hiller, *Clues for flavor from rare lepton and quark decays*, *JHEP* **06** (2015) 072 [arXiv:1503.01084] [INSPIRE].

[49] R. Alonso, B. Grinstein and J. Martin Camalich, *Lepton universality violation and lepton flavor conservation in B-meson decays*, *JHEP* **10** (2015) 184 [arXiv:1505.05164] [INSPIRE].

[50] L. Calibbi, A. Crivellin and T. Ota, *Effective field theory approach to $b \to s\ell\ell^{(')}$, $B \to K^{(*)}\nu\overline{\nu}$ and $B \to D^{(*)}\tau\nu$ with third generation couplings*, *Phys. Rev. Lett.* **115** (2015) 181801 [arXiv:1506.02661] [INSPIRE].

[51] R. Barbieri, G. Isidori, A. Pattori and F. Senia, *Anomalies in B-decays and $U(2)$ flavour symmetry*, *Eur. Phys. J.* **C 76** (2016) 67 [arXiv:1512.01560] [INSPIRE].

[52] M. Blanke and A. Crivellin, *B meson anomalies in a Pati-Salam model within the Randall-Sundrum background*, *Phys. Rev. Lett.* **121** (2018) 011801 [arXiv:1801.07256] [INSPIRE].

[53] G. Bélanger, C. Delaunay and S. Westhoff, *A dark matter relic from muon anomalies*, *Phys. Rev.* **D 92** (2015) 055021 [arXiv:1507.06660] [INSPIRE].

[54] S.M. Boucenna et al., *Non-abelian gauge extensions for B-decay anomalies*, *Phys. Lett.* **B 760** (2016) 214 [arXiv:1604.03088] [INSPIRE].

[55] S.M. Boucenna et al., *Phenomenology of an $\mathrm{SU}(2) \times \mathrm{SU}(2) \times U(1)$ model with lepton-flavour non-universality*, *JHEP* **12** (2016) 059 [arXiv:1608.01349] [INSPIRE].

[56] W. Altmannshofer, S. Gori, M. Pospelov and I. Yavin, *Quark flavor transitions in $L_\mu - L_\tau$ models*, *Phys. Rev.* **D 89** (2014) 095033 [arXiv:1403.1269] [INSPIRE].

[57] S. Descotes-Genon, L. Hofer, J. Matias and J. Virto, *Global analysis of $b \to s\ell\ell$ anomalies*, *JHEP* **06** (2016) 092 [arXiv:1510.04239] [INSPIRE].

[58] T. Hurth, F. Mahmoudi and S. Neshatpour, *On the anomalies in the latest LHCb data*, *Nucl. Phys.* **B 909** (2016) 737 [arXiv:1603.00865] [INSPIRE].

JHEP06(2019)089

[59] W. Altmannshofer, C. Niehoff, P. Stangl and D.M. Straub, *Status of the $B \to K^* \mu^+ \mu^-$ anomaly after Moriond 2017*, *Eur. Phys. J.* **C 77** (2017) 377 [arXiv:1703.09189] [INSPIRE].

[60] LHCb collaboration, *Measurement of the $B_s^0 \to \mu^+ \mu^-$ branching fraction and search for $B^0 \to \mu^+ \mu^-$ decays at the LHCb experiment*, *Phys. Rev. Lett.* **111** (2013) 101805 [arXiv:1307.5024] [INSPIRE].

[61] CMS, LHCb collaboration, *Observation of the rare $B_s^0 \to \mu^+ \mu^-$ decay from the combined analysis of CMS and LHCb data*, *Nature* **522** (2015) 68 [arXiv:1411.4413] [INSPIRE].

[62] ATLAS collaboration, *Study of the rare decays of B_s^0 and B^0 mesons into muon pairs using data collected during 2015 and 2016 with the ATLAS detector*, *JHEP* **04** (2019) 098 [arXiv:1812.03017] [INSPIRE].

[63] LHCb collaboration, *Measurements of the S-wave fraction in $B^0 \to K^+ \pi^- \mu^+ \mu^-$ decays and the $B^0 \to K^*(892)^0 \mu^+ \mu^-$ differential branching fraction*, *JHEP* **11** (2016) 047 [*Erratum ibid.* **04** (2017) 142] [arXiv:1606.04731] [INSPIRE].

[64] CDF collaboration, *Updated branching ratio measurements of exclusive $b \to s \mu^+ \mu^-$ decays and angular analysis in $b \to k^{(*)} \mu^+ \mu^-$ decays*, CDF public note 10894 (2012).

[65] CMS collaboration, *Angular analysis and branching fraction measurement of the decay $B^0 \to K^{*0} \mu^+ \mu^-$*, *Phys. Lett.* **B 727** (2013) 77 [arXiv:1308.3409] [INSPIRE].

[66] CMS collaboration, *Angular analysis of the decay $B^0 \to K^{*0} \mu^+ \mu^-$ from pp collisions at $\sqrt{s} = 8$ TeV*, *Phys. Lett.* **B 753** (2016) 424 [arXiv:1507.08126] [INSPIRE].

[67] LHCb collaboration, *Differential branching fractions and isospin asymmetries of $B \to K^{(*)} \mu^+ \mu^-$ decays*, *JHEP* **06** (2014) 133 [arXiv:1403.8044] [INSPIRE].

[68] BaBar collaboration, *Measurement of the $B \to X_s l^+ l^-$ branching fraction and search for direct CP-violation from a sum of exclusive final states*, *Phys. Rev. Lett.* **112** (2014) 211802 [arXiv:1312.5364] [INSPIRE].

[69] F. James and M. Roos, *Minuit: a system for function minimization and analysis of the parameter errors and correlations*, *Comput. Phys. Commun.* **10** (1975) 343 [INSPIRE].

[70] D. Straub, *flavio v0.11*, http://dx.doi.org/10.5281/zenodo.59840 (2016).

[71] Belle-II collaboration, *The Belle II physics book*, arXiv:1808.10567 [INSPIRE].

[72] J. Aebischer et al., *B-decay discrepancies after Moriond 2019*, arXiv:1903.10434 [INSPIRE].

JHEP06(2019)089